A&A manuscript no.
(will be inserted by hand later)

Your thesaurus codes are:
08.05.1, 09.03.1, 09.08.1, 09.09.1, 09.11.1

ASTRONOMY AND ASTROPHYSICS
19.6.1999

A near infrared study of the HII/photodissociation region DR 18 in Cygnus *

F. Comerón[1], **J. Torra**[2]

[1]European Southern Observatory, Karl-Schwarzschild-Strasse 2, D-85748 Garching bei München, Germany; fcomeron@eso.org
[2]Departament d'Astronomia i Meteorologia, Universitat de Barcelona, Av. Diagonal 647, E-08028 Barcelona, Spain; jordi@mizar.am.ub.es

Received; accepted

Abstract. Near infrared observations of DR 18, a HII region in the Cygnus X molecular complex, are presented in this paper. These observations reveal DR 18 as an arc-shaped nebula in the 2.2 μm region, with a central star of $V = 15.6$ obscured by $A_V \simeq 8$ magnitudes. Visible and near-infrared spectroscopy and photometry indicate a spectral type around B0.5V for this star, while a near-infrared color-color diagram of the stars in the area shows that the central star is the most luminous one of a loose aggregate. Analysis of the narrow band imaging in the K band suggests that the arc nebulosity is principally due to emission by small grains, heated by the central star, in a photodissociation region. We interpret the arc nebula as the interface between a molecular cloud that is being eroded by the central star and the resulting HII region. Using published models of photodissociation regions, we estimate the density in the arc nebula to be a few times 10^3 cm^{-3}. We briefly discuss the possible relation of the structures observed in the near infrared with the source IRAS 20333+4102, which has been included in several far infrared and radio studies of the area. We conclude that IRAS 20333+4102 is not directly related to any of the structures that we describe here, and could to be an intermediate mass protostar embedded deeper in the molecular cloud.

The emission associated to ionized gas in DR 18 has a morphology fairly different from that of the arc nebula, being brighter near the position of the central star. A crescent-shaped peak is observed beside the central star and facing the arc nebula, suggesting an interaction between a stream of ionized gas from the nebula and the wind from the central star. We present two dimensional gas dynamical simulations which successfully reproduce such gas stream, the bow shock ahead of the central star, and the overall appearance of the nebula. An essential component of our model is the existence of an outward-decreasing density stratification in the cloud being eroded, as is commonly observed in dense molecular clumps.

The simple geometry of the nebula and the observability of the central star at short wavelengths make the derivation of the physical conditions of the region and the modeling of its dynamical evolution comparatively easier than in other, similar regions. DR 18 thus provides a good case study of several features associated to the interaction of an early B star with a molecular cloud.

Key words: Stars: early type; ISM: clouds, HII regions, kinematics and dynamics, individual objects: DR 18

1. Introduction

The Milky Way in Cygnus offers one of the finest displays of large scale structures related to star forming activity in our Galaxy, mostly due to the fact that the line of sight runs approximately along the local spiral arm in this direction (Bochkarev & Sitnik 1985, Odenwald 1989, Odenwald & Schwarz 1993). One of the dominant features of this area is Cygnus X, a giant molecular complex containing numerous thermal and non-thermal arcminute-sized sources (see Wendker et al. 1991, and references therein) which reveal the existence of both embedded and emerged HII regions in different evolutionary stages, as well as supernova remnants, thus indicating a vigorous present and past massive star forming activity.

Among the HII regions of Cygnus X is DR 18 (Downes & Rinehart 1966), a rather inconspicuous object at visible wavelengths which so far has received relatively little attention. In visible light pictures of the area, DR 18 appears as a small ($\sim 1'$), amorphous patch of nebulosity surrounding a $V = 15.6$ star. However, the morphology

Send offprint requests to: F. Comerón

* Based on observations collected at the German-Spanish Astronomical Center (Calar Alto, Spain), and at the European Southern Observatory (La Silla, Chile)

becomes more interesting at infrared wavelengths, as revealed by the new observations that we present here. DR 18 appears as a distinctly arc-shaped nebula in the H and K bands, while narrow band infrared imaging suggests that most of the emission in that wavelength arises in a photodissociation region (PDR) outlining the interface between the HII region and the adjacent molecular cloud being eroded. The simple geometry of the PDR, and the fact that most of its illumination is produced by a single star which can be directly observed at visible and near-infrared wavelengths, makes DR 18 a promising target for further studies of the structures produced by the interaction of stellar ultraviolet radiation with a molecular cloud, as well as the chemical processes inside them.

In this paper we present and discuss our broad and narrow band observations of the DR 18 nebula in the J, H, and K windows, and their implications on the nature of the region. We also present JHK photometry of stars in the area, which reveals a loose cluster of young stars to which the one which ionizes the region probably belongs, and spectra of the ionizing star in the visible and in the 2 μm region. Finally, a comprehensive gas dynamical simulation accounting for the observed features is proposed.

In Section 2 we describe our observations. The results are presented in Section 3, and discussed in Section 4. A summary is given in Section 5.

2. Observations

The near infrared observations reported in this paper were carried out between 3 and 13 July 1998 using MAGIC, the near-infrared camera and spectrograph of the German-Spanish Astronomical Center on Calar Alto, Spain, mounted at the 1.23 m telescope. Additional observations in the visible could be obtained in an earlier run with the same telescope in Calar Alto, and spectroscopy of the central star in the visible was performed using the ESO New Technology Telescope in La Silla, Chile, in April 1999.

2.1. Near-infrared imaging and photometry

The images presented here are centered on the position of the star ioinizing the DR 18 nebula (hereafter referred to as "the central star"), $\alpha(2000) = 20^{\rm h}35^{\rm m}07\overset{\rm s}{.}0$, $\delta(2000) = +41°13'12''$. The pixel scale of MAGIC at the 1.23 m telescope is $1.145''$ pixel^{-1}, with each individual 256×256 frame covering 23.9 arcmin^2 on the sky. Individual sequences of images were obtained in each filter, with each sequence consisting of a raster of 3×3 points defining a $10'' \times 10''$ square grid. Sixty individual exposures of 1 sec were stacked together at each raster position. Upon completion of each raster, an area of the sky near DR 18 field but farther from the Milky Way was observed to obtain a sky frame. The sky frames were constructed by median averaging and deviant pixel clipping of images obtained on a five-point raster. After sky subtraction and flat fielding, the target frames were shifted to compensate for the telescope offset between raster positions and combined, with rejection of the highest and lowest pixel value at each point of the combined image to remove bad pixels and cosmic rays in the original images. Image reduction was performed using standard IRAF tasks and dedicated scripts.

In addition to the broad band observations in the J (1.25 μm), H (1.65 μm), and K (2.2 μm) filters, images were obtained as well in narrow band filters ($\Delta\lambda/\lambda = 1\%$) centered on the wavelenght of the (1,0) H_2 $S(1)$ line at 2.122 μm, the Brγ line at 2.166 μm, and the (2,1) H_2 $S(1)$ line at 2.248 μm. Moreover, observations were also obtained through a "CO-continuum" filter centered at 2.260 μm, used for another observing program executed during another part of the night. Having ($\Delta\lambda/\lambda = 3\%$), the CO continuum filter actually includes the entire passband of the (2,1) H_2 $S(1)$ filter. The total exposure times were 18 min for the J, H, and K filters; 36 min for the 2.122 μm and 2.248 μm filters; and 54 min for the 2.166 μm and 2.260 μm filters.

Digital photometry was carried out on the J, H, and K images in order to construct color-magnitude and color-color diagrams of the stars in the area, which may make it possible to identify very young stars possibly associated with the DR 18 HII region. The tasks in the DAOPHOT package layered on IRAF were used to identify the stars, adjust the point spread function, and perform digital photometry. The instrumental photometry was calibrated by observing the nearby infrared standard HD 203856 (Elias et al. 1982).

2.2. Near-infrared spectroscopy

We obtained a spectrum of the central star of DR 18 in the K-band window using a 2 pixel slit and the JK grism. The resulting spectrum has a resolution of $R = \lambda/\Delta\lambda \simeq 260$. To obtain it, we took several sequences of five individual spectra moving the star along the slit between each pair of exposures, in order to enable the removal of detector defects. The reduction of the spectra was carried out by means of IRAF scripts which used tasks in the NOAO/ONEDSPEC and TWODSPEC packages. One-dimensional spectra were extracted, combined, and wavelength-calibrated using the OH airglow lines as a wavelength reference (Oliva & Origlia 1992). Telluric absorption features were removed by ratioing the spectra by those of the nearby star HD 196850, whose G0 spectral type indicates the practical absence of any noticeable features in this wavelength domain, with the exception of a faint Br γ line (Kleinmann & Hall 1986). This star was observed inmediately after each observation of the central star of DR 18, at nearly the same airmass. Given the availability of time, a spectrum was also obtained of the brightest star of the field in the K band.

2.3. Imaging in the visible

Images of DR 18 in the V band and Hα were obtained by combining exposures obtained with the CCD camera at the 1.23 m telescope in September 1996. These observations were carried out under less than ideal conditions, but they are useful to compare the near-infrared and visible morphologies of the object, as well as to measure the visible magnitude of the central star. The latter was calibrated by observing the standard star HD 197037.

2.4. Spectroscopy in the visible

Spectra of the central star of DR 18 were obtained on 20 and 21 April 1999, using EMMI in low-resolution spectroscopy mode at the the 3.5 m ESO New Technology Telescope (NTT). Grism #3 was used in combination with a $2''$ slit, yielding a resolution of $R = \lambda/\Delta\lambda \simeq 350$. The rather wide slit, oriented following the parallactic angle, was chosen due to the degraded image quality resulting from the low altitude at which DR 18, a mid-northern object, has to be observed from La Silla. Three spectra obtained with the described setup were added together, totalling 60 min. of exposure time. Wavelength calibration was performed using a Th-Ar lamp. Relative flux calibration was achieved by ratioing the extracted spectra, corrected for atmospheric extinction, by the throughput curve of the system as previously determined by the team operating the NTT.

3. Results

3.1. Structure of the nebula

Images of DR18 in Hα and the J, H, and K bands are presented in Figure 1. At J, the overall appearance of the nebulosity matches well that observed in Hα, with the emission peaking near the position of the central star. The morphology changes in the H band, where the nebula is bounded to the East (left) by a bright rim. This is most clearly seen in the K band image, where the bright rim becomes the most prominent feature in the nebula. Faint filamentary extensions of the nebula cab also be seen towards the North and the East.

Narrow band images of the nebula in the 2 μm window, shown in Figure 2, can provide additional insights on the nature of the emission in different areas of the nebula. The bright rim dominates the emission in both of the images centered on the H_2 transitions, as well as in the broader band image centered at 2.26 μm. Fainter emission is seen in these filters in the parts of the nebula closer to the central star, but it is the Brγ emission which dominates in this region. The overall appearance of the nebula in Brγ is similar to that seen in the J band. The main morphological difference between the images centered on the two H_2 transitions is the fact that the outer edge of the arc-shaped nebula is outlined by a maximum in the (1,0) H_2 $S(1)$ image, which does not appear in any of the two other narrow filter images. In both the 2.248 μm and 2.260 μm filters, the intensity tends to increase towards the inner edge of the arc. Concerning the comparison between the 2.248 μm and 2.260 μm images one may expect that, if the nebula emitted most of the luminosity seen in those bands in the (2,1) H_2 $S(1)$ line, the threefold increase in filter width would imply a decrease of the brightness ratio of the nebula with respect to any star by a factor of 3 when passing from the 2.248 μm to the 2.260 μm filter. This is not what is seen in our images, where the brightness ratio of the nebula is seen to decrease slightly with respect to those of the stars, but by much less than a factor of 3. We take this as an indication that the dominant process responsible for the intensity observed in these bands is continuum emission, rather than emission in the (2,1) H_2 $S(1)$ line.

To better appreciate the structure of the nebulosity, especially in the proximities of the central star, we have artificially removed the stars in all the images. This was done using some of the utilities available in DAOPHOT: first, the task PSTSELECT was used to select a set of suitable reference stars for the determination of the point spread function, which was subsequently calculated using the task PSF. Stellar images were then located in each frame using the task DAOFIND, and the scaled point spread function at the position of each one was subtracted using the task ALLSTAR. The results are shown in Figure 3. The most dramatic effect of the subtraction of the stellar images takes place in the Brγ filter, in which removal of the central star reveals a bright crescent of emission peaking about $6''$ east of it. Such a peak is absent in the other narrow band images, but can also be identified in the Hα, J, and H band images. Given that intense hydrogen recombination lines fall in the latter two bands, it seems clear that this maximum is mostly due to recombination line emission.

Approximate flux calibration of the narrow band images has been performed by assuming that the flux emitted by the field stars is the same in all the narrow band filters, and the same in turn as the flux derived from the K band photometry. By using different box sizes around the nebula in the star-subtracted images, we estimate that the nebular integrated fluxes measured in this way have accuracies of ~ 20 % or worse. The integrated flux values obtained for the different filters are 0.38 Jy at 2.122 μm, 0.45 Jy at 2.166 μm, 0.40 Jy at 2.248 μm, and 0.29 Jy at 2.26 μm. While the quoted accuracy is too low for significative line ratios to be derived from these numbers, we take these results as a confirmation that the flux recorded in the different images is indeed dominated by the continuum, although with a significant contribution from H_2 and HI lines.

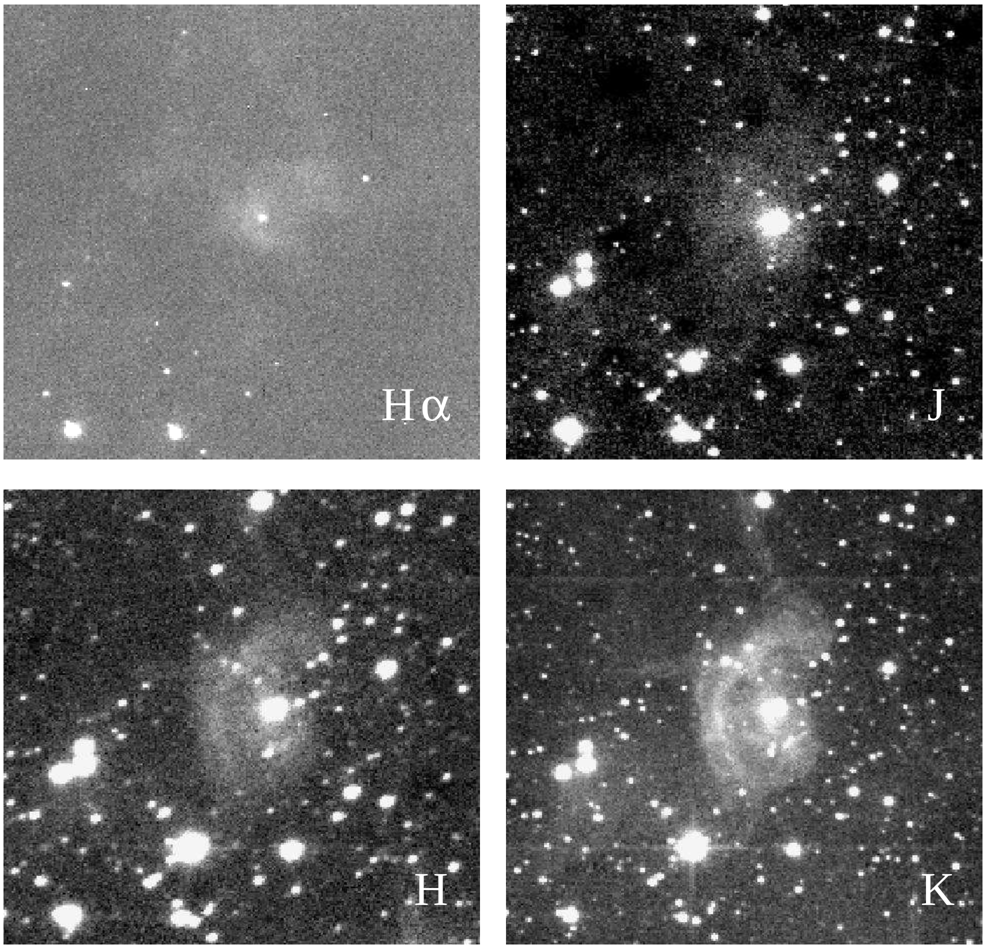

Fig. 1. Images of DR 18 in Hα and the J, H, and K filters. Each image is $4\farcm1 \times 3\farcm9$ in size. North is at the top and East on the left.

3.2. Spectra of the central star

Figure 4 shows the spectrum of the central star in the K window. For the sake of comparison, we show as well the spectrum of the brightest star appearing in the south-eastern quadrant of the K band image. The spectrum of the central star appears featureless at the resolution and signal-to-noise ratio used here. The absence of even Brγ in the spectrum shown here is however an artifact of the reduction: as mentioned in Section 2.2, the bright star used for the correction of telluric absorption is also expected to show Brγ absorption, and therefore this feature cancels out when ratioing both spectra. The reduced spectrum of the central star thus implies that its Brγ absorption has a similar equivalent width to that of a G0 star. We can in fact measure this absorption in the spectrum shown in the lower panel of Figure 4, which clearly corresponds to that of a reddened early M-type giant (Kleinmann & Hall 1986). Since its Brγ absorption should be negligible, the false emission appearing in its reduced spectrum at 2.166 μm is actually the reversed Bγ absorption of the star used for telluric correction. The measured equivalent width of this feature in the spectrum of the M star, $W(\mathrm{Br}\gamma) \simeq 4$Å, thus gives indirectly the equivalent width of Brγ in the spectrum of the central star. In the spectral classification scheme in the 2 μm region developed by Hanson et al. 1996, this value is typical of a main sequence star with a spectral type between $\sim$ O8 and B2. The absence of any other obvious lines in the spectrum is consistent with this classification. The slope of the spectrum over the K window may be due to a combination of foreground reddening and intrinsic excess emission in this spectral region. As discussed in Section 3.3, both effects are likely to be present in this object.

The spectral type can be better constrained using the visible spectrum presented in Figure 5. Because of the large foreground extinction, the blue part of the spectrum, where most of the features used for classification are found, has a poor signal-to-noise ratio. Nevertheless, the spectrum can be shown to be later than O-type due to the absence of the HeII line at 5411 Å. On the other hand, the HeI line at 4428 Å is clearly seen, with a depth similar to that of the Hγ line at 4340 Å, indicating a very

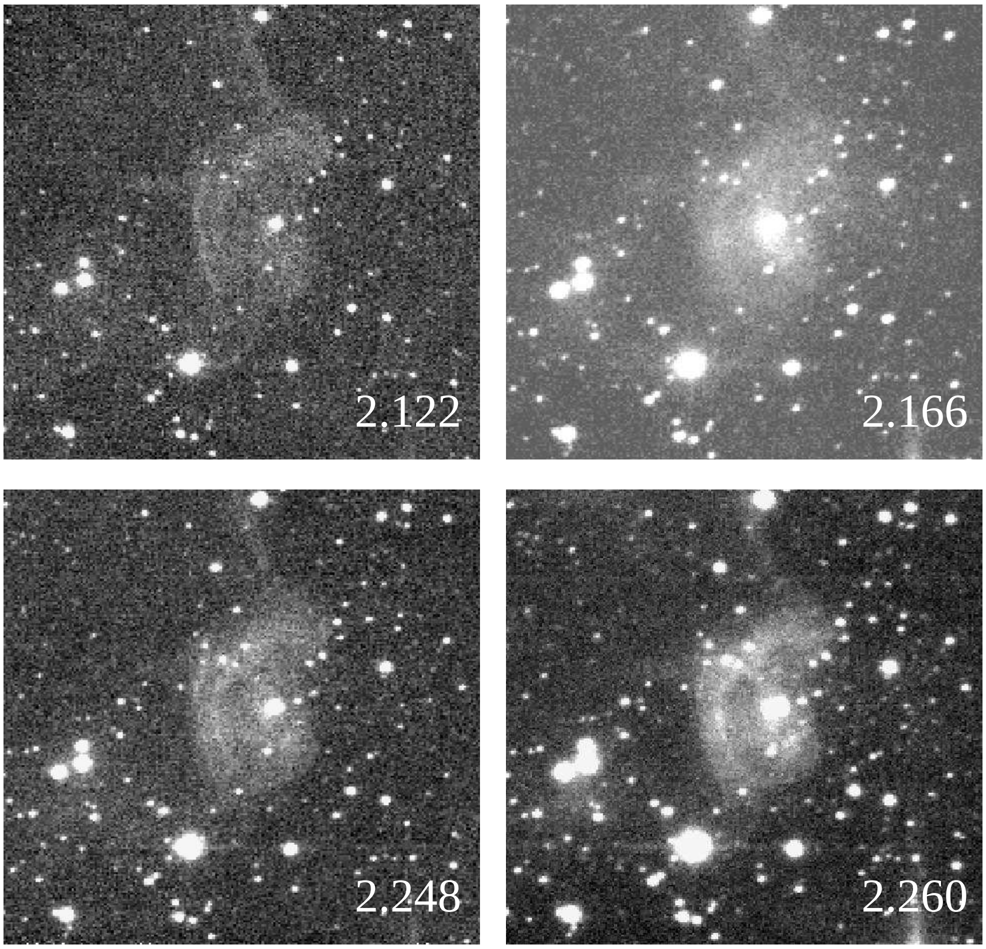

Fig. 2. Images of DR 18 in four narrow band filters in the K band. The 2.122 μm filter is centered on the (1,0) H_2 $S(1)$ line; 2.166 μm, on the Brγ line; 2.248 μm, on the (2,1) H_2 $S(1)$ line; and 2.260 μm, on a region used to measure the CO continuum in cool stars, which in this case includes also the (2,1) H_2 $S(1)$ line. The size and orientation are the same as in Figure 1.

early B type. We therefore classify the central star as B0-B1 (see Jacoby et al. 1984 for an atlas of stellar spectra at a similar resolution and covering a similar wavelength interval). Note also the appearance of strong interstellar lines, due to the high extinction towards the star, which include the diffuse interstellar band (DIB) features at 5780 Å and 6284 Å, as well as the Na I D doublet at 5890 Å, whose strength is usually observed to be similar to that of the 5780 Å feature (Dorschner et al. 1977). Using band strength to reddening ratios observed towards other lines of sight (Jenniskens et al. 1994) we find that the equivalent widths of these features, ~ 3 Å, are consistent with an extinction of ~ 8 mag toward the star, as discussed in Section 4.2.

3.3. Photometry

The near-infrared color-color diagram is a useful tool to discern young stellar objects from the unrelated background and foreground population, thanks to the excess emission displayed by stars still surrounded by circumstellar disks. By modeling the disk surrounding an intermediate mass star, such as a Herbig Ae/Be star, Lada & Adams 1992 showed that these objects occupy a region of the $(J-H)$, $(H-K)$ that is inaccessible to normal photospheres reddened by foreground extinction. Objects occupying that region of the diagram are thus likely to be in the early stages of their evolution. Since this is most likely to be the case of the central star illuminating the nebulosity of DR 18, the $(J-H)$, $(H-K)$ diagram has the potential of revealing fainter, roughly coeval companions that may have formed together with the central star, thus allowing a better understanding of the star formation process in the DR 18 region. The census of young stars obtained in this way may be incomplete for several reasons. Some of them may have already dissipated their disks, or may have an insufficient amount of circumstellar material close to the star for it to emit significantly at 2 μm. Moreover, stars heavily obscured by foreground dust would be missed at J, and it would not be possible to place them in the color-color diagram. Therefore, it must be kept in

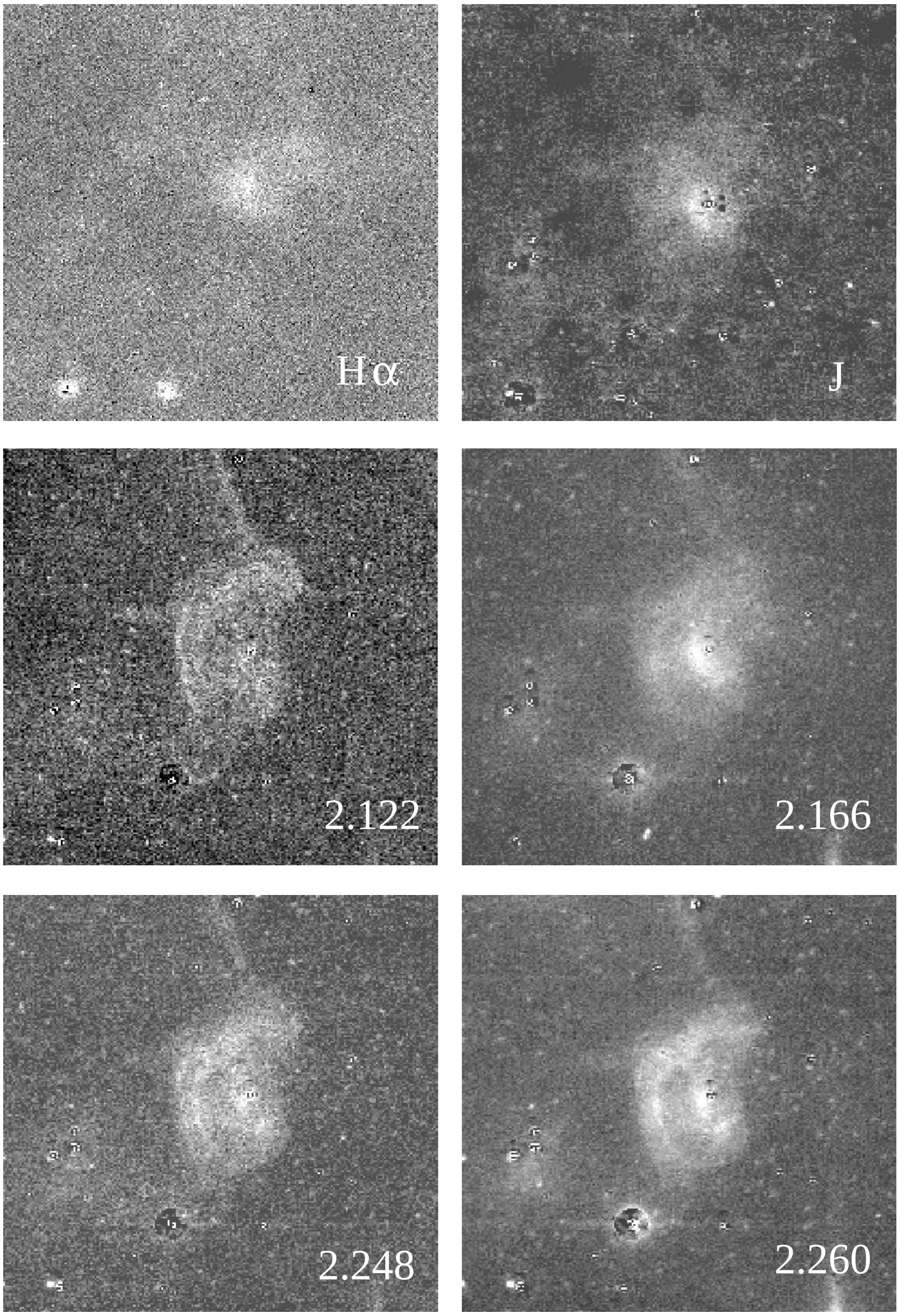

Fig. 3. A selection of broad and narrow band images in which the stellar images have been artificially subtracted using the method described in the text. Some residuals are still seen at the positions of the brightest stars. The size and orientation are the same as in Figure 1.

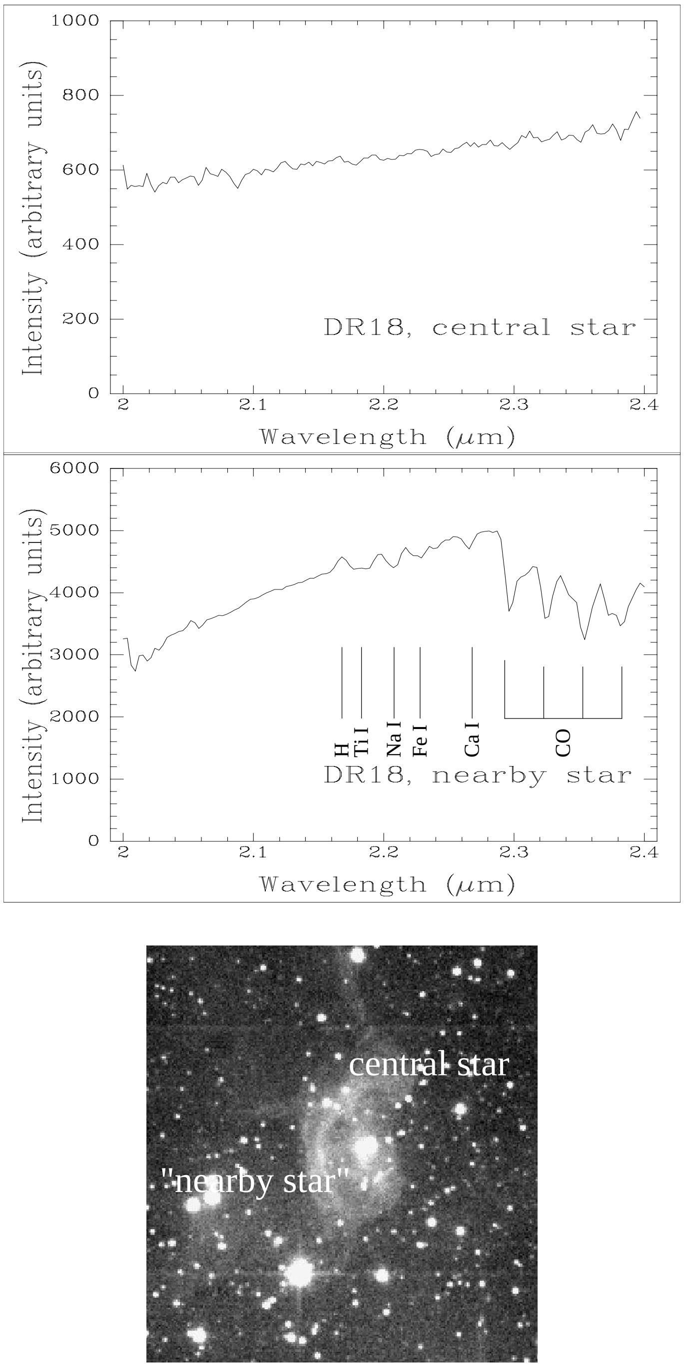

Fig. 4. Spectra of the DR 18 central star and the brightest star in K in the same field (here called the "nearby star"). Both stars are marked in the K band image under the two spectra. The principal spectral features visible in the spectrum of the nearby star, that we classify as an early M type supergiant, are indicated. The Brγ feature was not removed from the spectrum of the star used to correct for telluric absorption; this artificially suppresses the Brγ feature in the spectrum of the central star, and makes a false emission feature appear in the spectrum of the nearby star.

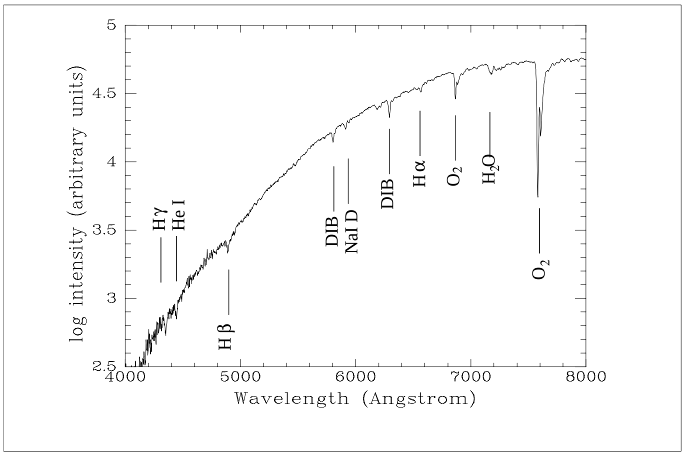

Fig. 5. Spectrum of the DR 18 central star at visible wavelengths, with the main stellar and interstellar features identified. The bands marked as O_2 and H_2O are telluric. The steep slope in the blue is a consequence of heavy extinction. Note that the vertical scale is logarithmic.

mind that the sample of young stars identified in this way is likely to be biased towards objects with large amounts of circumstellar material lying in regions of relatively low extinction.

The definition of the region of infrared excesses requires the adoption of a reddening vector. Although the near-infrared extinction law has been observed to be more universal than at visible wavelengths (Mathis 1990), departures are sometimes observed in star forming regions. The slope of the redening vector in the $(J-H)$, $(H-K)$ diagram, $E[J-H]/E[H-K]$, tends to decrease in such regions as the total-to-selective absorption ratio $R_V = A_V/E[B-V]$ increases, what is commonly interpreted as an effect of increased grain size. Thus, in the ρ Ophiuchi cloud, where $R_V \simeq 4.0$ (Vrba et al. 1993), $E[J-H]/E[H-K]$ is found to be 1.57 (Kenyon et al. 1998), as compared to the standard values of 3.1 and 1.7 (Rieke & Lebofsky 1985). Similarly, Wilking et al. 1997 find $E[J-H]/E[H-K] = 1.5$ in the star forming region around R Coronae Australis, where $R_V \simeq 4.4$ (Vrba & Rydgren 1984). However, this behavior may not be general: in Chamaeleon I, another star forming region with a R_V larger than average ($R_V \simeq 5$; Steenman & Thé 1989), Comerón et al. 1999 find a $(J-H)$, $(H-K)$ diagram where the distribution of objects, almost entirely composed of background stars, traces a reddening vector with $E[J-H]/E[H-K] = 1.7$ and is incompatible with a slope as low as 1.5. In the Cygnus region, Terranegra et al. 1994 find $R_V = 4.0$, but Torres-Dodgen et al. 1991 find $R_V = 3.04$ in the direction of Cygnus OB2, which is only 30' away from DR 18.

Figure 6 shows the color-color diagram of the stars in the imaged area. Only stars with $J < 17.5$, $H < 16.0$, $K < 16.0$ were retained to ensure color indexes accurate to

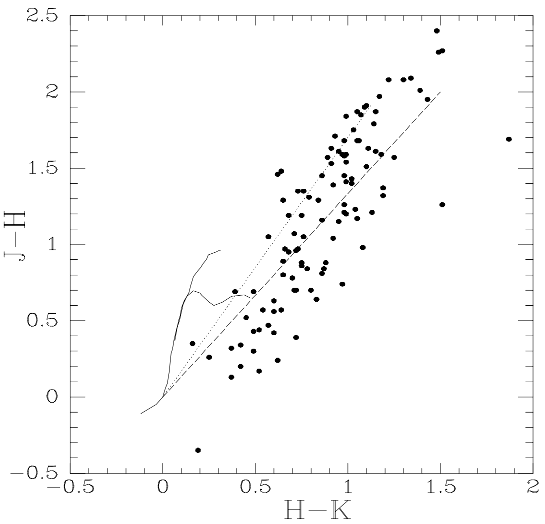

Fig. 6. Color-color diagram of the stars detected in the J, H, and K bands. The solid curves are the loci occupied by normal main sequence (lower branch) and giant stars (upper branch) (Bessell & Brett 1988). The dotted line is the reddening vector of the normal reddening law (Rieke & Lebofsky 1985), and the dashed line is a reddening vector with a slope of 1.5, as observed in some star forming regions.

0.1 mag. The solid curves are the loci populated by unreddened main sequence stars and giants (Bessell & Brett 1988). The straight lines are limiting reddening vectors with $E[J-H]/E[H-K] = 1.7$ and $E[J-H]/E[H-K] = 1.5$, according to the discussion in the previous paragraph. Their origin is placed at the intrinsic colors of an A0 star, as those would be the stars for which extinction would cause the reddest $(H-K)$ at a given $(J-H)$; for any reasonable slope of the reddening vector, M giants should always have a smaller $(H-K)$ than reddened A stars with the same $(J-H)$. This argument is not strictly true if the slope of 1.7 is adopted for the reddening vector, as unreddened late M dwarfs would be even redder in $(H-K)$. However, M dwarfs should be far too faint to be detected at the distance of DR 18.

The distribution of stars in the color-color diagram shows that the field is dominated at low extinctions by sources with K-band excess, regardless of the adopted extinction law. The interpretation at higher extinctions critically depends on the slope of the reddening vector: a slope of 1.7 places nearly all highly obscured objects in the zone of circumstellar excesses, a situation that we judge very unlikely. A slope of 1.5 is however consistent with the vast majority of objects with $(J-H) > 1.3$ being reddened background stars. The upper envelope of the distribution of points in Figure 6 is in agreement with the 1.5 slope, as no stars lie in the region above it, which should be inaccessible to stars both with and without circumstellar material. Therefore, in view of the distribution of stars in the $(J-H)$, $(H-K)$ diagram, we believe that a value of $E[J-H]/E[H-K] = 1.5$ is favoured.

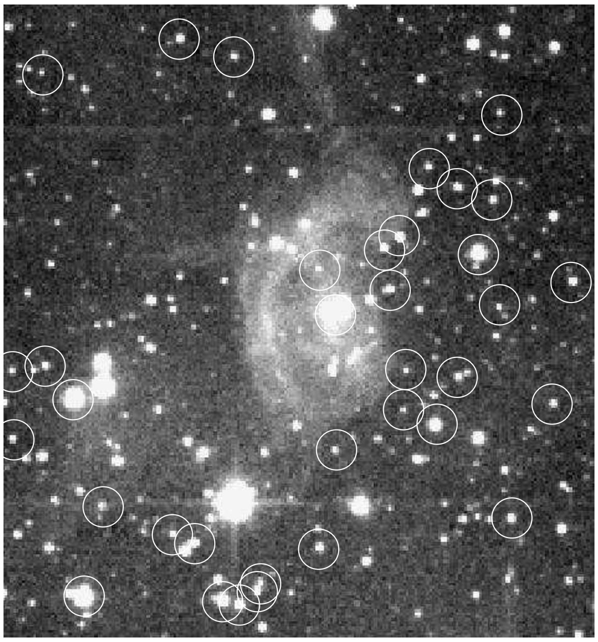

Fig. 7. Spatial distribution of the stars in the field of DR 18 appearing in the infrared excess region of Figure 6. The stars lying more than 0.2 mag to the right of the limiting reddening vector with slope 1.5 in that figure are surrounded by a circle in this K-band image.

The spatial distribution of the sources with infrared excess is presented in Figure 7. In it, sources having an observed $(H-K)$ color more than 0.2 mag redder than the limiting reddening vector at their $(J-H)$ position are marked on the K-band image. The inhomogeneity in their distribution is apparent, and a weak trend for them to lie along a band running from the southeast to the northwest may be appreciated. The scarcity of sources with infrared excess in the northeastern quadrant of the images is partly an obvious consequence of the lower observed overall density of sources in that area. This may in turn be caused by a higher extinction, confirmed by the fact that the objects with the reddest colors are generally found in that quadrant. However, a closer analysis of the data shows that the inhomogeneity of the overall distribution is accentuated when only infrared excess sources are taken into account, what we take as an evidence for a real clustering of such sources in the western and southern halves of the field. The central star of DR 18 thus appears to be the brightest member of a loose aggregate of young stars, with the less luminous members possibly illuminating the filaments extending to the North and to the East of the arc nebula. A wider area JHK survey reaching to similar magnitude limits as the one presented here should easily confirm or disprove the spatial distribution of sources hinted here.

4. Discussion

4.1. Previous studies of the DR 18 region

Despite the lack of near infrared observations of DR 18 in the literature, a number of surveys in the far infrared and radio domains have included it. The HII region has been observed in several hydrogen radio recombination lines (Piepenbrink & Wendker 1988, Lockman 1989). In the centimeter radio continuum, both single dish (Wendker 1984, Wendker et al. 1991) and aperture synthesis observations (Miralles et al. 1994) exist. At other wavelengths, studies have searched for emission by high density tracers such as H_2O masers (Scalise et al. 1989, Palla 1991, Brand et al. 1994, Miralles et al. 1994), NH_3 (Miralles et al. 1994, Molinari et al. 1996), HCO^+ (Richards et al. 1987) and H_2CO (Piepenbrink & Wendker 1988).

Many of the observations have been motivated by the presence in the region of IRAS 20333+4102, a point source in the IRAS catalog lying on a ridge of extended emission running from Southeast to Northwest. The IRAS colors of the point source are typical of a dense molecular core containing an embedded bright source (Wood & Churchwell 1989; Palla et al. 1991). Its fluxes in the (1,1) and (2,2) NH_3 lines (Miralles et al. 1994, Molinari et al. 1996) indicate a high temperature of 20 - 30 K, supporting the existence of an embedded source in a core with density $> 10^4 - 10^5$ cm^{-3}. Such densities are confirmed by the detection of HCO^+ (Richards et al. 1987). Even higher densities are revealed by the H_2O maser emission detected by Scalise et al. 1989, with an intensity of 5 Jy. Likely variability of the H_2O emission explains its non detection in other epochs, as reported in Brand et al. 1994 and Miralles et al. 1994, despite detection limits as low as 1.3 Jy rms. Nearly all the line measurements are coincident in assigning a velocity $V_{LSR} \simeq 7 - 10$ km s^{-1}, including the NH_3, HCO^+, H_2CO, and hydrogen recombination lines. The exception is the H_2O observation of Scalise et al. 1989, who found $V_{LSR} = -25.7$ km s^{-1}. This discrepancy is interpreted by Miralles et al. 1994 as being indicative of the existence of an outflow associated to the central object.

The precise position of IRAS 20333+4102 in our images is not known, as the beam sizes of IRAS and of the radio telescopes used for the observations of high density tracers are typically of a few arcminutes. However, a direct relation between the central star and IRAS 20333+4102 seems clearly discarded. The central star lies outside the IRAS error ellipse of that source, and all the high density tracers suggest its identification with a protostellar core, rather than with an emerged star. If the IRAS position is taken at face value, IRAS 20333+4102 lies $\sim 30''$ east of the central star, on the bright rim seen in the nebulosity in the K band. No obvious near-infrared counterpart of this source is identified, although a few very red sources with $(H-K) > 1.5$ exist within the IRAS error ellipse. The presence of IRAS 20333+4102 and the significant background emission prevents an estimate of the emission characteristics of the arc nebula at IRAS wavelengths.

The compact HII radio continuum emission detected in the VLA observations of Miralles et al. 1994 nicely matches in both position and appearance the crescent-shaped bright spot seen next to the central star in our Brγ image, which seems clearly related to the central star. This, together with the evolutionary scenario that we propose for DR 18 (see Section 4.3) naturally explains the offset between the IRAS position and the radio continuum peak remarked by Miralles et al., at least for the present case (such offsets have been observed by those same authors in a few other instances, but it is doubtful that the present cause applies to them as well). In this context, IRAS 20333+4102 may thus be an embedded source, perhaps an intermediate mass protostar (Molinari et al. 1996), embedded in the molecular cloud that is being eroded by the central star, bearing no direct relevance to the structures that are seen in the near infrared. Therefore, we will not include it in our further discussion of the region.

4.2. The central star and the distance to DR 18

Kinematic distances in the Cygnus region are very poorly constrained. The observed positive V_{LSR} of the material associated to the HII region and to IRAS 20333+4102 clearly places DR 18 in the Cygnus arm, rather than in the background Perseus arm where strongly negative velocities are observed. However, kinematic distances are meaningless for distances below $r \sim 3$ kpc, due to the small value of $|dV_{LSR}/dr|$. Using optical tracers, several authors have discussed distances to individual structures in the direction of Cygnus, finding in general values between 0.7 and 2.5 kpc for objects in the local arm (see e.g. Odenwald & Schwartz 1993). Discussing distances to OB associations possibly related to the Cygnus Superbubble, Comerón et al. 1993, 1998 adopt 1.25 kpc for the bulk of the massive stellar population, although a large scatter is certainly allowed by the available data.

Table 1. Observed and derived parameters of the central star

V	15.6 ± 0.1
J	10.63 ± 0.05
H	10.24 ± 0.05
K	9.52 ± 0.05
spectral type	B0.5 ± 0.5
A_V	8.1 ± 0.5 mag
distance	1.6 ± 0.4 kpc

A more precise determination of the distance is possible using the available $VJHK$ photometry of the central star and its spectral type, that we estimated to be between B0 and B1 as discussed in Section 3.2. The input photometry, and the estimated parameters that we discuss in this Section, are presented in Table 1. As a starting point, we have estimated the foreground extinction using the $(V-J)$ color, assuming that the flux at both bands is purely photospheric. This is a doubtful assumption for a young hot star at J, as circumstellar emission may be noticeable at this band. However, the moderately red $(J-H)$ and $(H-K)$ colors lead us to think that this is a reasonable approach. The extinction is then calculated as

$$A_V = \frac{(V-J)-(V-J)_0}{1-(A_J/A_V)} \tag{1}$$

where $(V-J)_0$ is the intrinsic color index, and A_J/A_V is given by the interstellar extinction law. Intrinsic color indexes for main sequence stars of spectral types B and later are compiled by Kenyon & Hartmann 1995. The $(V-J)_0$ color changes from -0.70 to -0.61 between types B0V and B1V. As to A_J/A_V, Rieke & Lebofsky 1985 give a value of 0.282 for the standard extinction law. Steenman & Thé 1989 have modelled the grain size distribution to account for anomalous extinction laws, and by increasing the maximum grain size to account for a total to selective extinction ratio $R_V = 4.1$ they predict $A_J/A_V = 0.33$. As discussed in Section 3.3, the extinction towards DR 18 may be expected to lie between these two cases. Considering all the possible values that can be obtained in Eq. (1) by varying $(V-J)_0$ and A_J/A_V between the quoted limits, we obtain that A_V most probably lies between 7.6 and 8.6. This source of uncertainty on the distance can be considered to be small, as we will estimate the latter using the J band flux, where the extinction (and its uncertainty) are reduced by a factor of 3. The luminosity of the star should lie between $\log L = 4.72$ for type B0V and $\log L = 4.20$ for type B1V (Schmidt-Kaler 1982) which, using the intrinsic color indexes and bolometric corrections of Kenyon & Hartmann 1995, translates into an absolute magnitude M_J between -3.28 (B0V) and -2.55 (B1V). In this way, we obtain for the distance r:

$$r = 10^{0.4(J-M_J+5-A_J)} = 1.6 \pm 0.4 \text{ kpc} \tag{2}$$

4.3. The nebula

4.3.1. Overall structure

The most remarkable feature of DR 18 in the near infrared is its distinct arc shape, and the changing appearance of the nebula in the different filters as seen in Figure 3 is essential to understand the nature of the emission. The brightness of the arc relative to the rest of the nebula is highest in the K band, and especially in the filters containing H_2 transitions (2.122 μm, 2.248 μm, and 2.260 μm). On the other hand, such a contrast is hardly seen in the J and 2.166 μm filters, where hydrogen recombination lines are expected to dominate (Paβ in the J band, and Brγ in 2.166 μm). The overall appearance of the nebula, even excluding the prominent knot of emission near the central star, is rather centrally peaked in those bands. This suggests that the brightness enhancement in the arc is not directly related to the HII region, although the arc can still be traced in the J and 2.166 μm filters all the way out to nearly its outer rim. In the H band image (Figure 2) the situation is intermediate: the bright rim can still be discerned, although it is not as prominent as in the K band. The H window is expected to contain abundant hydrogen recombination lines, corresponding to transitions of the Brackett series from levels higher than 10.

4.3.2. The photodissociation region

Additional information on the nature of the emission from the arc can be obtained from the fact, already noted in Section 3.1, that the intensity ratios between the 2.248 μm and the 2.260 μm images are approximately the same for the stars as for the nebula, suggesting that, like in the stars, the nebular emission is mostly in the form of a continuum, at least at those wavelengths. Such continuum emission must provide a nonzero background in all the narrow band filters, including Brγ, to be taken into account when considering the spatial distribution of the ionized gas. Near infrared continuum emission is frequently seen in reflection nebulae illuminated by early B stars (Sellgren 1984, Sellgren et al. 1992, Giard et al. 1994, Field et al. 1998), as well as in planetary nebulae (Likkel et al. 1994, Hora et al. 1993, Luhman & Rieke 1996). Several possible origins for it have been proposed. Models based on the transient heating of very small grains ~ 10 Å in size by the ultraviolet emission from the star (Sellgren 1984) successfully account for the spectral energy distribution of this continuum emission, characterized by a color temperature of $\sim 1,000$ K. Other sources of continuum can be macromolecules such as polycyclic aromatic hydrocarbons (PAHs; Giard et al. 1994). Black & van Dishoeck 1987 also note that the blending of the very numerous fluorescence lines arising in radiatively excited H_2 produces a pseudo-continuum when observed at low spectral resolution. However, the latter explanation seems unlikely in the present case, as an intense pseudo-continuum would be accompanied by even more intense emission in the main fluorescence lines, what is not supported by the comparison between the 2.248 μm and the 2.260 μm images as noted above. Moreover, the pseudocontinuum should be more intense at J, while the arc is actually almost inobservable in that band. The increasing prominence of the arc towards longer wavelengths also argues against scattered starlight as the origin of the luminosity (Sellgren et al. 1992). An explanation for the continuum emission based on either small grains or PAHs thus seems the most likely one.

The inner edge of the arc can then be explained as due to either a front of destruction of the emitting particles, or to a density discontinuity. The latter is expected to take place in the transition layer from cold neutral gas to an HII region as a consequence of the large difference in temperature, provided that the ionized gas is allowed to expand rapidly. Moreover, if the emitting particles are PAHs, the first cause would be present too: as shown by Giard et al. 1994, PAHs are destroyed in a very short timescale after crossing the ionization front. Both explanations thus place the ionization front at the inner edge of the arc shaped nebula. The fact that a peak is observed in the 2.248 μm and 2.260 μm images, and more faintly in the 2.122 μm image, near the position of the central star (although by far not as prominent as the 2.166 μm peak) suggests that the particles responsible for the continuum emission do survive in the HII region environment. Thus, we tentatively ascribe the continuum emission to small heated grains. The absence of the PAH 3.3 μm feature in future spectroscopic observations of the crescent-shaped peak would confirm this hypothesis.

If the continuum emission of the arc nebula is mostly due to small grains or large molecules in the zone inmediately outside the HII region, such emission can thus be considered as a tracer of the PDR that constitutes the interface between it and the unperturbed molecular gas that the central star is eroding. The remarkable regularity of the PDR suggests that the molecular gas belongs to a single clump with a well defined structure, rather than to a complex of clumps; in the latter case, the ultraviolet radiation would be expected to penetrate to widely varying depths, resulting in a more extended and irregular emission, as is observed in other regions (Schneider et al. 1998). Models of PDR emission in the near infrared have concentrated on the predicted spectrum of fluorescent emission by H_2 (Black & van Dishoeck 1987, Abgrall et al. 1992, Draine & Bertoldi 1996; see also the comprehensive review on H_2 infrared emission mechanisms by Sternberg 1989, and references therein). Our images do not allow the direct observation of H_2 emission or the measurement of line ratios, but some theoretical results concerning the thickness of the PDR can provide useful insights on its physical conditions.

We use for this purpose the extensive set of models calculated by Black & van Dishoeck 1987. We are mainly interested in the ratio of the derived column density of photodissociated gas to the input volume density of the models. This ratio should provide an estimate of the geometrical depth of the PDR, which can be directly measured in our images and, for a given density, it depends primarily on the intensity of the incident ultraviolet radiation at $\lambda > 912$ Å. Realistic limits on the radiation field thus constrain the volume density in the PDR. To estimate the incident flux per unit surface of the arc nebula, we have used the ultraviolet spectrophotometry of Holberg et al. 1982 for ϵ Per, a star commonly classified as B0.5V (e.g. Murphy 1969). The distance has been taken as 165 pc from the *Hipparcos* parallax. From the ultraviolet spectrum of Holberg et al. 1982, we take the flux at 1000 Å as 700 photons cm^{-2} s^{-1} Å^{-1}. This corresponds to 4.8×10^8 photons cm^{-2} s^{-1} Å^{-1} at the estimated distance of 0.2 pc between the star and the inner surface of the arc nebula, assuming a negligible absorption of photons with $\lambda > 912$ Å in the HII region. At 1000 Å, this is $\sim 4 \times 10^3$ times the background ultraviolet field in the solar neighbourhood adopted by Black & van Dishoeck 1987. The thickness of the PDR at the adopted distance to DR 18, $\simeq 0.1$ pc, thus places rather strong constraints on the density: Model 13 of Black & van Dishoeck predicts that thickness for $n_H = 3 \times 10^3$ cm^{-3} and an ultraviolet flux 10^2 greater than the interstellar average, while their Model 20, in which $n_H = 10^4$ cm^{-3}, requires an ultraviolet flux 100 times higher to produce the same geometrical depth. Given the calculated ultraviolet flux of the central star as seen from the inner edge of the nebula, a crude estimate of the volume density in the arc nebula is $\sim 5 \times 10^3$ cm^{-3}. As found by Black & van Dishoeck 1987, this estimate is fairly sensitive to the grain properties and the formation model of H_2 molecules. Moreover, the inferred column density, of order 10^{21} cm^{-2}, is in the range where line overlap becomes important in the treatment of radiative transfer inside the PDR (Draine & Bertoldi 1996), and a more realistic treatment may result in a decrease of the estimated density. On the other hand, the model results depend little on the temperature of the PDR (Black & van Dishoeck 1987) and on the color temperature of the ultraviolet radiation field (Bertoldi & Draine 1996). Dynamical effects resulting from the presence of an ionization front propagating into the PDR are unlikely to be important in the case of moderate ultraviolet fields, like the one produced by the central star of DR 18 (Bertoldi & Draine 1996).

The dominance of the continuum emission prevents us from carrying out a more detailed analysis based on line ratios, and future K-band spectroscopy of DR 18 may be expected to substantially improve the assessment of its physical conditions on the basis of a detailed comparison to PDR models. Given the passbands of the narrow band filters used in our imaging (Section 2.1), the continuum would dominate over the emission in the (1,0) H_2 S(1) line in other objects described in the literature, such as the Orion bar PDR (Luhman et al. 1998), the planetary nebula Hubble 12 (Luhman & Rieke 1996), and probably other planetary nebulae as well (Likkel et al. 1994). However, judging from Burton et al. 1998, narrow-band imaging at 2.122 μm of NGC 2023 may be dominated by line emission, although probably not everywhere (see Field et al. 1998). As to DR 18, the eastern outer rim of the arc nebula may be an exception to the overall dominance of the continuum emission. Figures 2 and 3 show that this rim is brightened in the 2.122 μm images, a feature that is not seen in any other of the narrow band filters, including the one centered at 2.248 μm. We interpret this as due to the (1,0) H_2 $S(1)$ line being much stronger with respect to the local continuum than in other parts of the nebula. This is what would be expected if the PDR is bounded in the side opposite to the central star by a shock that propagates into the molecular cloud. Collisional excitation may thus be the dominant mechanism of excitation of H_2 in this region, while past the shock and closer to the star it would be ultraviolet pumping. If this is so, then the shock must be faster than ~ 5 km s^{-1} in order to heat the gas to the $\sim 10^3$ K required to populate the $v = 1$ level of the H_2 molecules (Shull & Draine 1987, Sternberg 1989). The absence of enhanced (2,1) H_2 $S(1)$ emission in the 2.248 μm filter is consistent with a non dissociative shock, rather than ultraviolet pumping, as the mechanism producing the H_2 emission in that layer. Using the relation for the Alfvén velocity $v_A(\mathrm{km\ s^{-1}}) = 22\ B(\mathrm{mG})\ n(\mathrm{cm^{-3}})^{-1/2}$ (Genzel 1992) and the empirical scaling relationship for the magnetic field $B(\mu\mathrm{G}) = n(\mathrm{cm^{-3}})^{1/2}$ (Troland & Heiles 1986), the quoted minimum velocity of 5 km s^{-1} would be weakly superalfvénic, although whether or not this is really so obviously depends on the actual values of the density and the magnetic field. A shock velocity of 5 km s^{-1} can thus be considered as a lower limit, while a velocity above ~ 50 km s^{-1} would produce a dissociative shock increasing the $(1,0)/(2,1)$ ratio to a value of order unity, which is not observed.

4.3.3. The ionized gas

The emission peak near the central star seen in the J and the 2.166 μm bands, as well as in the centimeter continuum as pointed out in Section 4.1, suggests the interaction of a flow of ionized gas streaming away from the arc nebula with the environment of the central star. This is supported by the crescent shape of the peak, and by its orientation facing the nebula. Such flow of ionized gas is expected to occur naturally when a molecular cloud is being ionized by a star located outside it (Tenorio-Tagle et al. 1979), and some actual examples of it have been observed (e.g. the HII region S 201; Felli et al. 1987). If the star has a considerable wind and is conveniently placed, it may act as an obstacle in the stream of ionized gas, which then forms a crescent-shaped density enhancement ahead of the star.

The erosion of a cloud by a star located outside it may be regarded as a particular case of the *champagne* phase of a HII region (Tenorio-Tagle & Bodenheimer 1988, and references therein). A common feature to the dynamical simulations of the classical *champagne* phase, in which the star lies within or near a cloud of uniform density, is the acceleration of gas to supersonic velocities in a transition zone, lying between the compact HII region contained in the volume initially occupied by the molecular cloud, and the extended component originated by the ionized material expanding in the intercloud medium. Therefore, in this scenario the ionizing star should be placed in the outskirts of this transition zone or in the extended component in order to develop a bow shock around it.

This does not seem to be the case for DR 18, where the star lies approximately on the major axis of an ellipse roughly delineating the arc nebula. This may be just an effect of perspective if the star happened to be projected in front or behind the arc, but physically far from the molecular cloud. However, in such case we should be seeing the bow shock nearly pole-on, approximately surrounding the star rather than beside it. Moreover, the supersonic region in the *champagne* model for a cloud of uniform density has a density much lower than that of the ionized gas in the compact component, and the bow shock would then produce just a very slight increase on the background emission caused by the compact component. The observations suggest that the acceleration of the gas to supersonic velocities thus takes place in the compact component.

To explore the conditions under which a bow shock like the observed one would develop, while being consistent with the observed morphology of the emission and the position of the central star, we have performed several gas dynamic numerical simulations suited to the specific conditions of DR 18. The methods used are based on those described by Comerón 1997 to study the erosion of a molecular cloud by an embedded star, taking into account the effects of both the ionizing radiation and the stellar wind. The 2-D computations have been carried out on an grid of 400×400 cells simulating the axial plane of a cylinder 0.5 pc in height and 0.5 pc in radius, with a linear resolution of 0.0013 pc, and assuming symmetry around the axis. Due to the complexity involved in modeling the physical conditions inside it, we have made no attempt at reproducing the PDR in the simulations.

We have carried out an initial set of simulations placing the star at different locations with respect to the boundary of a cloud of uniform density, both inside and outside it. The reference parameters used for the star are a mass loss rate $\dot{M}_w = 10^{-7}$ M$_\odot$ yr^{-1} and a terminal wind velocity $v_w = 200$ km s^{-1}. These are rather arbitrary choices, but our conclusions on the formation of a bow shock are unchanged when varying either of the two parameters even by a factor of 10. The ionizing flux of the star has been set to 10^{47} photons s^{-1} (Schaerer & de Koter 1997); again, reasonable changes in this value do not affect our results. The density of the cloud has been varied between 5×10^3 and 10^4 cm^{-3}. Our results confirm those of Tenorio-Tagle and collaborators in that the flow of gas around the star is very slow when it is placed inside the cloud, and no bow shock develops. On the other hand, placing the star in the region of supersonic flow does produce a bow shock as expected, but in a region where the ambient density of ionized gas is typically a factor of 4 or more smaller than in the compact component contained in the cloud. Since the geometrical depth of the compact component (roughly given in our case by the size of the ring nebula) is much greater than that of the bow shock, the latter would be indistinguishable in practice.

We have found a much better agreement with the observations when allowing the density of the cloud to increase with depth. This is expected to be closer to the reality, in agreement with observations of the structure of clumps within molecular clouds which typically have density profiles $\rho \propto r^{-2}$ (e.g. Williams et al. 1995). In the present case, IRAS 20333+4102 may be a protostar being formed at the high density center of the core. If the ionizing star is placed off-center, the density gradient inside the cloud becomes a pressure gradient when the gas is ionized, which produces supersonic motions of ionized gas inside the compact component.

This is illustrated by the results of the numerical simulation shown in Figure 8. The input parameters of the simulation are as described above, but the molecular cloud is now modelled as a plane-parallel stratified slab with the density increasing from a value of 10^4 cm^{-3} at the surface of the cloud to infinity at the edge of the grid, following a $\rho \propto z^{-2}$ law (where z is the coordinate parallel to the axis). The star is initially placed near the edge of the cloud, 0.0125 pc below its surface. The upper panels in Figure 8 depict the distribution and motions of the gas 1.7×10^5 years after the onset of the ionizing flux and the stellar wind, when a sizeable cavity has been already produced in the cloud. The density gradient makes the ionization front propagate faster in the direction parallel to the surface of the molecular cloud, thus giving the HII region a bowl shape. We note that the edge of the DR 18 HII region, as outlined by the PDR, is also elongated, rather than hemispherical as would be in the case of the erosion of a homogeneous molecular cloud. The growth in the parallel direction is however moderated by the dense stream of ionized gas flowing outwards from deeper into the cloud, which maintains a high density ($\sim$ 300 cm^{-3} in the example shown here) in the cavity. The upper right panel in Figure 8, with the velocity map superimposed on the density contour plot, shows that the ionized gas is accelerated to supersonic velocities soon after being ionized. In the stage of evolution shown here, the gas moves at 15 km s^{-1} towards the star when it finds the bow shock caused by its interaction with the stellar wind. The structure produced by this interaction has been studied in detail by Comerón & Kaper 1998. The situation found here is comparable to the case of a low velocity runaway star described in that paper, giving rise to a stable bow shock.

The lower panel in Figure 8 simulates the spatial distribution of the emission measure, $\int n_e^2 \, dl$, where n_e is the electron density and l is the length along the line of sight. In a first approximation, this figure should thus be compared to the observed distribution of intensity. An angle of view of 45^0 formed by the visual and the axis of the computational grid has been assumed, being representative of

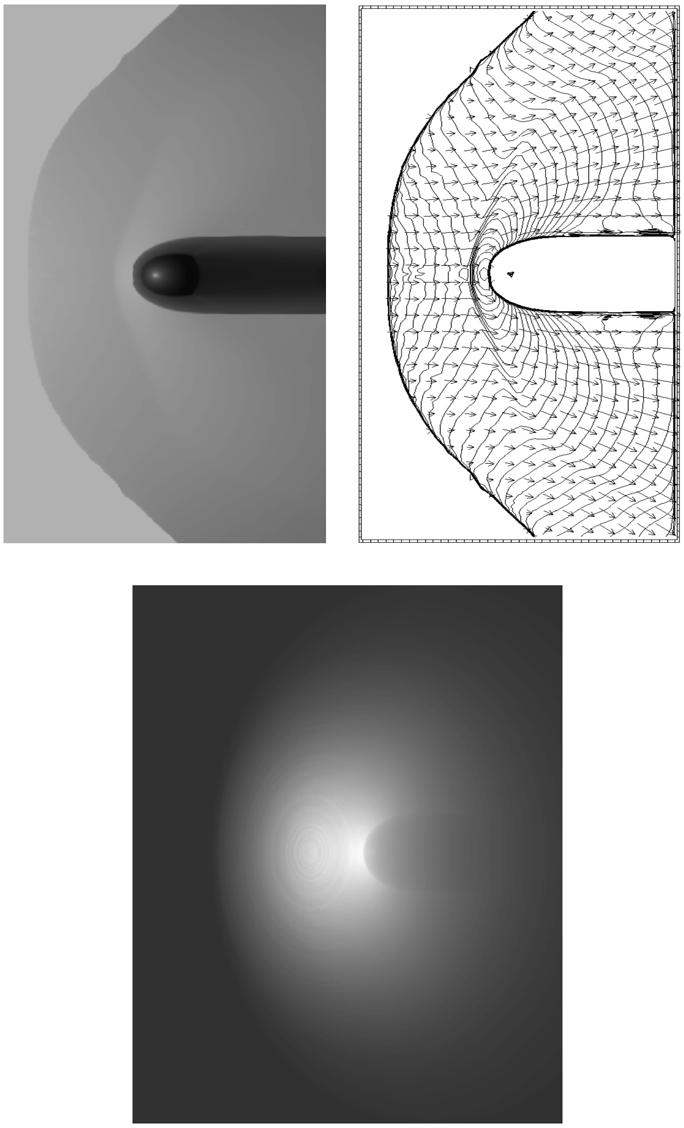

Fig. 8. Model structure of DR 18, using the input parameters described in the text, 1.7×10^5 years after the ionizing flux and the stellar wind are switched on. *Upper left:* Density structure of the ionized gas flow. To clearly show the formation of the bow shock, the greyscale on the left panel has been set so that white represents densities above 3000 cm^{-3}; the stratified molecular gas thus lies outside the greyscale used here. The density increase factor of the gas when crossing the bow shock is 2.15, and the maximum density in the bow shock is 700 cm^{-3}. *Upper right:* The velocity vector of the gas at different points of the grid is plotted on a contour map of the density. The longest vector shown represents a velocity of 20.5 km s^{-1}. *Bottom:* Distribution of the emission measure that would be observed along lines of sight forming an angle of 45° with respect to the axis of the simulation. A crescent shape appears just ahead of the star and facing the cloud, as observed in DR 18. The units are arbitrary; the ratio between the peak value and that at mid distance between the peak and the edge of the HII region is 1.7.

the results found over a fairly wide range of observation geometries. In agreement with the observations, the intensity distribution peaks just ahead of the star. This is due to the local increase in density caused by the compression of the gas in the bow shock, but also to the fact that such peak is seen in projection against a broader peak of emission due to the compact component. Finally, we note that the crescent shape is rather due to the sharp cut in intensity behind the star, where the dense ionized flow is replaced by a much more tenuous, hot gas produced by the collision between the stellar wind and the HII region. The numerical simulation presented here yields a ratio of 1.7 between the peak intensity and the intensity midway between the peak and the edge of the HII region, comparable to the 2.5 ± 0.3 that we estimate from our Brγ images. It should be kept in mind however that the images also contain a contribution from heated dust. The intensity distribution produced by small dust grains in the HII region is expected to peak near the star too, due to the increase in density found at the bow shock, but also to the higher rate of absorption of ultraviolet photons per grain. This effect is not taken into account in the numerical simulations, what prevents a straightforward comparison between the Brγ image and the simulated map of emision measure.

The description given here is mostly qualitative and does not intend to reproduce in detail the observed structure of the HII region. This is due to the many free input parameters of the simulations, to the limited constraints on the relevant quantities that can be derived from our observations, and to the entangling between the emission of small particles and of the ionized gas. However, the basic characteristics of the scenario described here remain valid when changing the input parameters (ionizing flux, stellar wind, cloud density and size) within a broad range.

5. Summary

In this paper we have presented near infrared observations of DR 18, a faint HII region in the Cygnus X molecular complex. The ionizing star is found to have an early B spectral type from both photometry and spectroscopy. Many lightly obscured stars in the imaged area occupy the area of the $(J-H)$, $(H-K)$ diagram that indicates the presence of considerable amounts of circumstellar material, suggesting that the ionizing star is the brightest member of a loose aggregate of young stars.

The near-infrared morphology of the nebula in the K band is markedly different from that at visible wavelengths, being dominated by a bright, thick arc. Near the position of the central star, a crescent-shaped peak in the emission is seen, most prominently in the bands containing recombination emission lines from hydrogen. This peak is also observed in aperture synthesis observations in the centimeter radio continuum. By considering the emission as seen in different narrow bands, we conclude that the arc nebula actually traces a photodissociation region, with most of the emission being produced by small grains transiently heated to high temperatures by the central star. The photodissociation region is the interface between a faint HII region ionized by the central star, and a nearby molecular cloud, in which the central star was probably born. The HII region is produced by the Lyman continuum flux of the central star as it dissociates and ionizes the molecular gas. The cloud contains an embedded source, IRAS 20333+4102, inconspicuous or invisible in the near infrared. This source does not appear to be playing so far any significant role in the structure and dynamics of the region as observed in the near infrared, and it is probably embedded in the cloud at a depth still unreached by the ionization front.

The ionized gas reaches its peak brightness in the proximity of the central star, on the side of it facing the nebula. The shape of this peak suggests the interaction of a flow of ionized gas away from the molecular cloud with the stellar wind from the star, in a version of the *champagne* phase of the evolution of a HII region. We have simulated this interaction by means of numerical gasdynamic simulations, and conclude that a density gradient must exist in the molecular cloud in order to produce supersonic velocities inside cavity digged by the ionizing radiation of the central star. The overall shape of the nebula, and the shape and position of the peak in the emission of ionized gas, are successfully accounted for by this model assuming a density profile of the cloud decreasing with the square of the distance to the center, as is commonly observed in molecular cores. We speculate that IRAS 20333+4102 may be a protostar being born at the center of this core.

DR 18 is an object with a simple geometry, in which the main components of the structure resulting from the erosion of a molecular cloud by a star with moderate ionizing flux can be readily discerned. The ionizing star itself can be easily studied spectroscopically, both in the visible and in the near-infrared. DR 18 thus provides a very useful example for the study of the chemical and dynamical processes taking place when molecular clouds are destroyed by stars at the faint end of the OB class, and it is an excellent target for follow-up multiwavelength observations probing in detail the different components that we have described in this work.

Acknowledgements. We are very grateful to Ms. Núria Domènech for her work on the reduction of an initial set of observations, which led to the first identification of the near-infrared morphology of DR 18. We are pleased to thank the staffs at Calar Alto and La Silla Observatories for their assistance during the observations, especially Mr. Manuel Alises and Mr. Felipe Hoyo in Calar Alto, and Mr. Hernán Núñez and Mr. Ariel Sánchez in La Silla. Dr. Kurt Birkle is thanked for kindly making available to us some of his observing time with the CCD camera at the 1.23 m telescope. The referee, Dr. M. van den Ancker, is thanked for his careful reading of the manuscript and insightful remarks. JT acknowledges support by the CICYT under contract ESP97-1803.

References

Abgrall, H., Le Bourlot, J., Pineau des Forêts, G., Roueff, E., Flower, D.R., Heck, L., 1992, A&A, 253, 525.
Bertoldi, F., Draine, B.T., 1996, ApJ, 458, 222.
Bessell, M., Brett, J.M., 1988, PASP, 100, 1134.
Black, J.H., van Dishoeck, E.F., 1987, ApJ, 322, 412.
Bochkarev, N.G., Sitnik, T.G., 1985, Ap&SS, 108, 237.
Brand, J., Cesaroni, R., Caselli, P., et al., 1994, A&AS, 103, 541.
Burton, M.G., Howe, J.E., Geballe, T.R., Brand, P.W.J.L., 1998, PASAu, 15, 183.
Comerón, F., 1997, A&A, 326, 1195.
Comerón, F., Kaper, L., 1998, A&A, 338, 273.
Comerón, F., Rieke, G.H., Neuhäuser, R., 1999, A&A, 343, 477.
Comerón, F., Torra, J., Jordi, C., Gómez, A.E., 1993, A&AS, 101, 37.
Comerón, F., Torra, J., Gómez, A.E., 1998, A&A, 330, 975.
Dorschner, J., Friedemann, C., Gürtler, J., 1977, A&A, 58, 201.
Downes, D., Rinehart, R., 1966, ApJ, 144, 937.
Draine, B.T., Bertoldi, F., 1996, ApJ, 468, 269.
Elias, J.H., Frogel, J.A., Matthews, K., Neugebauer, G., 1982, AJ, 87, 1029.
Felli, M., Hjellming, R.M., Cesaroni, R., 1987, A&A, 182, 313.
Field, D., Lemaire, J.L., Pineau des Forêts, G., Gerin, M., Leach, S., Rostas, F., Rouan, D., 1998, A&A, 333, 280.
Genzel. R., 1992, in "The galactic interstellar medium", eds. W.B. Burton, B.G. Elmegreen, R. Genzel, Springer-Verlag.
Giard, M., Bernard, J.P., Lacombe, F., Normand, P., Rouan, D., 1994, A&A, 291, 239.
Hanson, M.M., Conti, P.S., Rieke, M.J., 1996, ApJS, 107, 281.
Holberg, J.B., Forrester, W.T., Shemansky, D.E., Barry, D.C., 1982, ApJ, 257, 656.
Hora, J.L., Deutsch, L.K., Hoffmann, W.F., Fazio, G.G., Shivanandan, K., 1993, ApJ, 413, 304.
Hutsemékers, D., Van Drom, E., Gosset, E., Melnick, J., 1994, A&A, 290, 906.
Jacoby, G.H., Hunter, D.A., Christian, C.A., 1984, ApJS, 56, 257.
Jenniskens, P., Ehrenfreund, P., Foing, B., 1994, A&A, 281, 517.
Kenyon, S.J., Hartmann, L., 1995, ApJS, 101, 117.
Kenyon, S.J., Lada, E.A., Barsony, M., 1998, AJ, 115, 252.
Kleinmann, S.G., Hall, D.N.B., 1986, ApJS, 62, 501.
Lada, C.J., Adams, F.C., 1992, ApJ, 393, 278.
Likkel, L., Morris, M., Kastner, J.H., Forveille, T., 1994, A&A, 282, 190.
Lockman, F.J., 1989, ApJS, 71, 469.
Luhman, K.L., Rieke, G.H., 1996, ApJ, 461, 298.
Luhman, K.L., Engelbracht, C.W., Luhman, M.L., 1998, ApJ, 499, 799.
Mathis, J.S., 1990, ARA&A, 28, 37.
Miralles, M.P., Rodríguez, L.F., Scalise, E., 1994, ApJS, 92, 173.
Molinari, S., Brand, J., Cesaroni, R., Palla, F., 1996, A&A, 308, 573.
Murphy, R.E., 1969, AJ, 74, 1082.
Odenwald, S.F., 1989, AJ, 97, 801.
Odenwald, S.F., Schwartz, P.R., 1993, ApJ, 405, 706.
Oliva, E., Origlia, L., 1992, A&A, 254, 466.
Palla, F., Brand, J., Cesaroni, R., Comoretto, G., Felli, M., 1991, A&A, 246, 249.
Palla, F., Cesaroni, R., Brand, J., Caselli, P., Comoretto, G., Felli, M., 1993, A&A, 280, 599.
Piepenbrink, A., Wendker, H.J., 1988, A&A, 191, 313.
Richards, P.J., Little, L.T., Toriseva, M., Heaton, B.D., 1987, MNRAS, 228, 43.
Rieke, G.H., Lebofsky, M.J., 1985, ApJ, 288, 618.
Scalise, E., Rodríguez, L.F., Mendoza-Torres, E., 1989, A&A, 221, 105.
Schaerer, D., de Koter, A., 1997, A&A, 322, 598.
Schmidt-Kaler, Th., 1982, in Landolt-Börnstein, Vol. 2b, eds. J. Schaifers and H.H. Voigt, Springer-Verlag.
Schneider, N., Stutzki, J., Winnewisser, G., Poglitsch, A., Madden, S., 1998, A&A, 338, 262.
Sellgren, K., 1984, ApJ, 277, 623.
Sellgren, K., Werner, M.W., Dinerstein, H.L., 1992, ApJ, 400, 238.
Shull, J.M., Draine, B.T., 1987, in "Interstellar Processes", eds. D.J. Hollenbach and H.A. Thronson.
Steenman, H., Thé, P.S., 1989, Ap&SS, 189, 189.
Sternberg, A., 1989, in Proc. 22nd Eslab Symposium on infrared spectroscopy in astronomy, ESA SP-290.
Tenorio-Tagle, G., Bodenheimer, P., 1988, ARA&A, 26, 145.
Tenorio-Tagle, G., Yorke, H.W., Bodenheimer, P., 1979, A&A, 80, 110.
Terranegra, L., Chavarría, C., Diaz, S., González-Patiño, D., 1994, A&AS, 104, 557.
Torres-Dodgen, A.V., Carroll, M., Tapia, M., 1991, MNRAS, 249, 1.
Troland, T.H., Heiles, C., 1986, ApJ, 301, 339.
Vrba, F.J., Rydgren, A.E., 1984, ApJ, 283, 123.
Vrba, F.J., Coyne, G.V., Tapia, S., 1993, AJ, 105, 1010.
Wendker, H.J., 1984, A&AS, 58, 291.
Wendker, H.J., Higgs, L.A., Landecker, T.L., 1991, A&A, 241, 551.
Williams, J.P., Blitz, L., Stark, A.A., 1995, ApJ, 451, 252.
Wilking, B.A., McCaughrean, M.J., Burton, M.G., Giblin, T., Rayner, J.T., Zinnecker, H., 1997, AJ, 114, 2029.
Wood, D.O.S., Churchwell, E., 1989, ApJ, 340, 265.

This article was processed by the author using Springer-Verlag LaTeX A&A style file *L-AA* version 3.